Preprints of the 20th World Congress
The International Federation of Automatic Control
Toulouse, France, July 9-14, 2017

Output Feedback Stabilization of Inertial Stabilized Platform with Unmatched Disturbances Using Sliding Mode Approach ⋆

Jianliang Mao * **Jun Yang** * **Shihua Li** * **Qi Li** *

* *School of Automation, Southeast University, Key Laboratory of Measurement and Control of CSE, Ministry of Education,Nanjing 210096, China. (e-mail: lsh@seu.edu.cn).*

Abstract: Inertial stabilized platforms are extensively used to keep the light of sight free from the effects of vehicle motion or vibration. In order to reduce the assembly difficulty and cost as well as achieve an accurate pointing in the presence of disturbances, a finite-time output feedback control strategy is proposed. On the basis of the dynamic model with both matched and unmatched uncertainties, two high-order sliding mode observers are designed to estimate the newly defined virtual state and the lumped uncertainty, respectively. Combing with the nonsingular terminal sliding mode technique, an output feedback control based on the estimates and the output is developed. The proposed method can achieve not only stability and robustness against uncertainties but also the finite-time convergence to the desired angular rate without control chattering. Finally, the comparative simulations are performed to show the effectiveness of the proposed method.

Keywords: Inertial stabilized platform, output feedback control, high-order sliding mode observer, nonsingular terminal sliding mode, unmatched disturbances.

1. INTRODUCTION

Optical-electronic tracking system (OETS) is widely used in the military and civil field. In order to maintain the optical axis toward a moving target, inertial stabilized platform (ISP) is usually utilized to keep the light of sight (LOS) free from the effects of vehicle motion or vibration (Ekstrand, 2001; Hurák and Řezáč, 2012). However, the stabilized performance are always affected by various disturbed phenomena like cross-couplings, mass unbalance, parameter variations, and external wind-gust. High precision control has been an challenging task for ISP system in the presence of the mentioned multiple disturbances.

In order to make the LOS insensitive to disturbances, two decoupled single-input-single-output (SISO) controllers with cascaded structure are commonly developed for 2-degree-of-freedom (2-DOF) ISP system (Hurák and Řezáč, 2012). In this strategy, for each gimbal, two PI controllers are designed to stabilize the inertial angular rate and the motor current, respectively. There exist some limitations about the above configuration. From the mechatronic design point of view, at least three kinds of sensors are necessary for the signal measurements, i.e., optical encoder for the relative angle measurement, fiber optical gyro (FOG) for the inertial angular rate measurement, and hall sensor for the current measurement, which results in the growths of assembly difficulty and design cost. From the perspective of controller design, the subsistent time-varying disturbances can not be suppressed efficiently only with the traditional PI control. Some elegant control approaches, such as $H\infty$ control (Řezáč and Hurák, 2013), fuzzy control (Abdo et al., 2014) and internal mode control (Zhou et al., 2014) have been investigated to improve the control performance. However, these feedback control approaches can only attenuate the nonvanishing disturbances to some extent rather than completely remove them. Besides, additional available signals except the inertial angular rate are required for the controller design.

Output feedback regulator approach has provided an alternative way to compensate the effects of disturbances and uncertainties (Chen and Huang, 2005). In order to realize the controller design in the case that only the inertial angular rate is available, other states as well as disturbances of ISP system should be estimated by an observer primarily. The sliding mode observer is widely used due to its finite-time convergence performance and insensitivity to system uncertainties. It has been reported in Chalanga et al. (2016) that super-twisting observer (STO) is able to estimate the unknown state for double-integrator system in the presence of disturbances. Recently, high-order sliding mode observer (HOSMO) has been extensively investigated by many scholars (Levant, 2003; Basin et al., 2016; Dai et al., 2016). The above literature results imply that not only the system states but also the

⋆ This paper was supported by the foundation of International Science & Technology Cooperation Program of China (2015DFA10490), the National Natural Science Foundation of China (61473080), and the Fundamental Research Funds for the Central Universities and the Innovate Foundation for Graduate Student of JiangSu Province (KYLX15_0213).

disturbances can be precisely estimated in finite time by using HOSMO method.

In order to guarantee a fast convergence rate of system output, nonsingular terminal sliding mode (NTSM) control is widely studied since it can achieve finite-time stability without causing any singularity problem (Feng et al., 2002). However, it can only realize first-order sliding mode rather than SOSM, which causes the chattering phenomenon unavoidably. To realize the continuous action, finite-time control (FTC) method associating with NTSM is developed in Yu et al. (2005). But the tracking error can not be guaranteed to zero in the presence of model uncertainties and external disturbances. In addition, the system states must be measurable for the sliding-surface design.

In this paper, we propose a finite-time output feedback control strategy for 2-DOF ISP system. The system subject to multiple unmatched disturbances in the case of current and angle sensorless is considered. The dynamic model with both matched and unmatched uncertainties is established primarily. Two HOSMOs are designed to estimate the newly defined virtual state and the lumped uncertainty, respectively. In virtue of NTSM design technique, an output feedback controller based on the estimates and the output is constructed. Finite-time convergence proof is completed via Lyapunov stability theory. Finally, the comparative simulations are presented to show the effectiveness of the proposed method.

2. MODEL DESCRIPTION AND PROBLEM FORMULATION

The control frame of OETS is typically composed of three feedback control loops, i.e., tracking loop, stabilized loop, and current loop. To improve the dynamic response and the disturbance rejection ability, we focus on the controller design of stabilized loop and current loop in this paper. By fixing a 2-axis FOG on the inner gimbal (pitch-axis) of the ISP system, the stable control of LOS can be accomplished on both pitch and yaw channels, utilizing the gyro signals as the feedback. Permanent-magnet DC (PMDC) motors are applied as the direct drive devices due to their high torque when operating at a low speed.

To simplify the description, the coordinate definition stated in Ekstrand (2001) is adopted with no change. Three reference frames are introduced: the gimbal platform or base frame B, the gimbal mediator or outer frame K, and finally the inner frame A. For the angular rates of frames B, K, and A relative to inertial space, respectively, we introduce $\mathbf{\Omega_B}$, $\mathbf{\Omega_K}$, and $\mathbf{\Omega_A}$, where $\mathbf{\Omega_B} = [p, q, r]^{\mathrm{T}}$, $\mathbf{\Omega_K} = [p_k, q_k, r_k]^{\mathrm{T}}$, and $\mathbf{\Omega_A} = [p_a, q_a, r_a]^{\mathrm{T}}$, where p, q, and r are the components of the inertial angular rate vector in frame B, and the notations p, q, and r are for the roll, pitch, and yaw components, respectively, and similar definitions are made for the other vectors. The relative angles of yaw and pitch rotations are denoted as v_1 and v_2. Then the angular rate kinematics of two gimbals are given by

$$\mathbf{\Omega_K} = \mathbf{R_b^k} \cdot \mathbf{\Omega_B} + \begin{bmatrix} 0 \\ 0 \\ \dot{v}_1 \end{bmatrix}, \mathbf{\Omega_A} = \mathbf{R_k^a} \cdot \mathbf{\Omega_K} + \begin{bmatrix} 0 \\ \dot{v}_2 \\ 0 \end{bmatrix} \quad (1)$$

where $\mathbf{R_b^k}$ and $\mathbf{R_k^a}$ are the transformations from B to K and K to A, respectively, denoted as

$$\mathbf{R_b^k} = \begin{bmatrix} \mathbf{C}v_1 & \mathbf{S}v_1 & 0 \\ -\mathbf{S}v_1 & \mathbf{C}v_1 & 0 \\ 0 & 0 & 1 \end{bmatrix}, \mathbf{R_k^a} = \begin{bmatrix} \mathbf{C}v_2 & 0 & -\mathbf{S}v_2 \\ 0 & 1 & 0 \\ \mathbf{S}v_2 & 0 & \mathbf{C}v_2 \end{bmatrix} \quad (2)$$

where $\mathbf{S}$ and $\mathbf{C}$ denote sine and cosine functions, respectively. For 2-DOF ISP system, the inertial matrices of the gimbals are denoted as

$$\mathbf{J_A} = \begin{bmatrix} J_{ax} & D_{xy} & D_{xz} \\ D_{xy} & J_{ay} & D_{yz} \\ D_{xz} & D_{yz} & J_{az} \end{bmatrix}, \mathbf{J_K} = \begin{bmatrix} J_{kx} & d_{xy} & d_{xz} \\ d_{xy} & J_{ky} & d_{yz} \\ d_{xz} & d_{yz} & J_{kz} \end{bmatrix}. \quad (3)$$

Combining (1)-(3) together, the dynamic model of the pitch and yaw gimbal can be derived as

$$J_i(v_2, t)\dot{\omega}_i = T_{mi} - T_i(\omega_i, v_2, t) \quad (4)$$

where $i = q$ and r represent the pitch and yaw axes, respectively, $J_i(v_2, t)$ is the total moment of inertia imposed on the gimbal, ω_i is the inertial angular rate (i.e., $\omega_q = q_a, \omega_r = r_a$), T_{mi} is the total torque, including the electromagnetic torque T_{ei}, the friction torque $F_c(\dot{\theta}_i, t)$ where θ_i is the relative angle (i.e., $\theta_r = v_1, \theta_q = v_2$), and the unmodeled dynamics and external disturbances $D_i(\omega_i, t)$, and $T_i(\omega_i, v_2, t)$ represents the highly cross-coupling term. One can refer to Ekstrand (2001) for a detailed derivation.

It is accessible to get the nominal value J_{oi} of $J_i(v_2, t)$, i.e., $J_{oq} = J_{ay}, J_{or} = J_{az} + J_{kz}$, since $\Delta J_i = J_i(v_2, t) - J_{oi}$ can be considered as the parameter variations and treated as the model uncertainties. The electromagnetic torque is generated by the PMDC motor, which is denoted as $T_{ei} = k_{ti} i_{ai}$, where k_{ti} is the torque coefficient and i_{ai} is the armature current. The friction torque can be divided into a linear part $B_i\dot{\theta}_i$ and a nonlinear part $F_i(\dot{\theta}_i, t)$, where B_i is the viscous friction coefficient.

For the adopted PMDC motors, the voltage balance equation is presented as

$$L_{ai}\dot{i}_{ai} = V_i u_i - R_{ai} i_{ai} - k_{vi}\dot{\theta}_i \quad (5)$$

where L_{ai} is the armature inductance, V_i is the input DC voltage, u_i is the chopper duty cycle, R_{ai} is the armature resistance, and k_{vi} is the back-EMF coefficient.

Note that $\dot{\theta}_i$ commonly exists in (4) and (5), which can not be measured directly in practical case without an additional angle/velocity sensor. But we can calculate it by using (1) as

$$\begin{aligned} \dot{\theta}_q &= \dot{v}_2 = \omega_q - \Omega_q(\omega_q, v_2, t), \\ \dot{\theta}_r &= \dot{v}_1 = \omega_r - \Omega_r(\omega_r, v_2, t) \end{aligned} \quad (6)$$

where $\Omega_q(\omega_q, v_2, t) = q_k$ and $\Omega_r(\omega_r, v_2, t) = r_a - r_a \sec v_2 + p_k \tan v_2$, denoting the structured uncertainties. By submitting (6) into (4) and (5), we can obtain the second-order dynamic model as follows

$$\begin{aligned} \dot{\omega}_i &= -\frac{B_i}{J_{oi}}\omega_i + \frac{k_{ti}}{J_{oi}} i_{ai} + \frac{H_{1i}}{J_{oi}}, \\ \dot{i}_{ai} &= -\frac{k_{vi}}{L_{ai}}\omega_i - \frac{R_{ai}}{L_{ai}} i_{ai} + \frac{V_i}{L_{ai}} u_i + \frac{H_{2i}}{L_{ai}} \end{aligned} \quad (7)$$

where H_{1i} and H_{2i} represent the unmatched and matched lumped uncertainties, respectively, defined by

$$\begin{aligned} H_{1i} =& B_i\Omega_i(\omega_i, v_2, t) - F_i(\omega_i, t) - T_i(\omega_i, v_2, t) \\ & - D_i(\omega_i, t) + d_{1i}(\omega_i, t), \\ H_{2i} =& k_{vi}\Omega_i(\omega_i, v_2, t) + d_{2i}(\omega_i, t) \end{aligned} \quad (8)$$

where $d_{1i}(\omega_i, t)$ and $d_{2i}(\omega_i, t)$ denote the uncertainties caused by parameter variations of $J_i(v_2, t)$, B_i, k_{ti}, L_{ai}, V_i, R_{ai}, and k_{vi}. Note that the unmatched lumped uncertainty H_{1i} consists of cross-couplings, friction torque, parameter variations, and external disturbances, which has the negative impacts on the control accuracy of LOS. Consequently, it is imperative to counteract the adverse effects of the multiple disturbances for the high precision control.

In this paper, we consider the case that only the inertial angular rates q_a and r_a are measurable. By introducing a new state vector $[x_{1i}, x_{2i}]^{\mathrm{T}}$, where

$$\begin{aligned} x_{1i} =& \omega_i^* - \omega_i, \\ x_{2i} =& \dot{\omega}_i^* + \frac{B_i}{J_{oi}}\omega_i - \frac{k_{ti}}{J_{oi}} i_{ai} - \frac{H_{1i}}{J_{oi}}, \end{aligned} \tag{9}$$

and ω_i^* is the desired angular rate, system (7) can be rewritten as

$$\begin{aligned} \dot{x}_{1i} =& x_{2i}, \\ \dot{x}_{2i} =& F_{ri}(x_{1i}, x_{2i}) + b_i u_i + H_{di} \end{aligned} \tag{10}$$

where

$$\begin{aligned} &F_{ri}(x_{1i}, x_{2i}) = \ddot{\omega}_i^* + F_{2i}(\dot{\omega}_i^* - x_{2i}) + F_{1i}(\omega_i^* - x_{1i}), \\ &H_{di} = -\frac{R_{ai}}{J_{oi}L_{ai}} H_{1i} - \frac{k_{ti}}{J_{oi}L_{ai}} H_{2i} - \frac{1}{J_{oi}} \dot{H}_{1i}, \\ &F_{1i} = \frac{k_{ti}k_{vi} + R_{ai}B_i}{J_{oi}L_{ai}}, F_{2i} = \frac{B_i}{J_{oi}} + \frac{R_{ai}}{L_{ai}}, b_i = -\frac{k_{ti}V_i}{J_{oi}L_{ai}}. \end{aligned} \tag{11}$$

In the practical system, the desired value ω_i^* is given by the outer tracking loop (Hurák and Řezáč, 2012). The control task is to achieve a fast and accurate tracking performance for ISP system in the presence of multiple disturbances. To this end, this paper recommends a finite-time output feedback control based on sliding mode approach, which achieves not only stability and robustness against the uncertainty but also finite-time convergence to the desired angular rate without the control chattering.

3. CONTROLLER DESIGN

In this section, we will design a finite-time output feedback control based on NTSM surface and HOSMO.

3.1 Reaching-Law Based Sliding Mode Controller Design

If the uncertainty H_{di} is known and both states x_{1i} and x_{2i} are available, then we can develop a reaching-law based finite-time SOSM controller.

It is well known that the sliding mode design is divided into two steps. First, to ensure fast and accurate tracking performance, the fast terminal sliding mode reaching law (Yu et al., 2005) is employed to improve the dynamic responses of the states in reaching phase, which is designed as

$$\dot{s}_i = -\bar{\lambda}_{1i} s_i - \bar{\lambda}_{2i} |s_i|^{\beta_i} \mathrm{sign}(s_i) \tag{12}$$

where s_i is the sliding variable, $\bar{\lambda}_{1i} = k_i\alpha_i |x_{2i}|^{\alpha_i - 1}\lambda_{1i}$, $\bar{\lambda}_{2i} = k_i\alpha_i |x_{2i}|^{\alpha_i - 1}\lambda_{2i}$, and λ_{1i}, $\lambda_{2i} > 0$, and $0 < \beta_i < 1$ are the design parameters. Second, we choose the NTSM-type sliding surface (Feng et al., 2002), denoted as

$$s_i = x_{1i} + k_i |x_{2i}|^{\alpha_i} \mathrm{sign}(x_{2i}) \tag{13}$$

where $k_i > 0$ and $1 < \alpha_i < 2$ are the design parameters.

By differentiating the sliding surface (13), one can obtain that

$$\begin{aligned} \dot{s}_i =& x_{2i} + k_i\alpha_i |x_{2i}|^{\alpha_i - 1} \dot{x}_{2i} \\ =& x_{2i} + k_i\alpha_i |x_{2i}|^{\alpha_i - 1} [F_{ri}(x_{1i}, x_{2i}) + b_i u_i + H_{di}]. \end{aligned} \tag{14}$$

Combining with (13) and (14), the control law can be derived as

$$\begin{aligned} u_i =& -b_i^{-1}(u_{eqi} + u_{ni}), \\ u_{eqi} =& \frac{1}{k_i\alpha_i} |x_{2i}|^{2-\alpha_i} \mathrm{sign}(x_{2i}) + F_{ri}(x_{1i}, x_{2i}) + H_{di}, \\ u_{ni} =& \lambda_{1i} s_i + \lambda_{2i} |s_i|^{\beta_i} \mathrm{sign}(s_i) \end{aligned} \tag{15}$$

where u_{eqi} is an equivalent control law and u_{ni} is a reaching control law. Here the uncertainty H_{di} is precisely compensated in the design. In this case, we can obtain the following conclusion.

Theorem 1. If the sliding surface is chosen as (13) and the control law is designed as (15), then the angular rate ω_i converges to the desired value ω_i^* in finite time.

Proof. Consider the following Lyapunov function candidate $V_1(s_i) = 1/2 s_i^2$, taking the derivative of $V_1(s_i)$ yields

$$\begin{aligned} \dot{V}_1(s_i) =& s_i \dot{s}_i \\ =& -k_i\alpha_i |x_{2i}|^{\alpha_i - 1} (\lambda_{1i} s_i^2 + \lambda_{2i} |s_i|^{\beta_i + 1}) \\ =& -2\bar{\lambda}_{1i} V_1(s_i) - 2^{\frac{\beta_i + 1}{2}} \bar{\lambda}_{2i} V_1(s_i)^{\frac{\beta_i + 1}{2}}. \end{aligned} \tag{16}$$

For the case of $x_{2i} \neq 0$, there is $\bar{\lambda}_{1i}$ and $\bar{\lambda}_{2i} > 0$. It can be followed from Yu et al. (2005) that the sliding variable $s_i = 0$ after finite time T_{1i}. For the case of $x_{2i} = 0$, by submitting (15) into (10) we have

$$\dot{x}_{2i} = -\lambda_{1i} s_i - \lambda_{2i} |s_i|^{\beta_i} \mathrm{sign}(s_i). \tag{17}$$

If $s_i \neq 0$, one can obtain that $\dot{x}_{2i} \neq 0$, that is x_{2i} is not an attractor (Yu et al., 2005). Therefore, it can be concluded that the system states can reach the sliding surface in finite time.

Once the sliding surface $s_i = 0$ is reached, that is

$$x_{1i} = -k_i |\dot{x}_{1i}|^{\alpha_i} \mathrm{sign}(\dot{x}_{1i}). \tag{18}$$

From (18) we know that the system states x_1 and x_2 are finite-time stable. That is, finite-time convergence of tracking error between ω_i^* and ω_i is obtained. This completes the proof.

However, the uncertainty H_{di} is time-varying and unknown in reality. In addition, x_{2i} is also unknown since it contains the unmatched multiple disturbances $H_{1i}(t)$ and unavailable signal i_{ai}.

3.2 HOSMO Based Output Feedback Sliding Mode Controller Design

To handle the mentioned problems, motivated by Chalanga et al. (2016), two HOSMOs are designed to estimate the newly defined virtual state x_{2i} and the uncertainty H_{di}, respectively.

Before the controller design, the following assumption is made firstly.

Assumption 2. The second derivative of virtual state x_{2i} is existing and bounded by a positive constant L_{1i}. The lumped uncertainty H_{di} has a Lipschitz constant L_{2i}.

Due to the fact that $F_{ri}(x_{1i}, x_{2i})$ contains the unavailable state x_{2i}, the first HOSMO is designed to estimate x_{2i} as follows

$$I:\begin{cases}\dot{\hat{x}}_{1i} = v_{1i}, \dot{\hat{x}}_{2i} = v_{2i}, \dot{\hat{x}}_{3i} = v_{3i},\\ v_{1i} = \hat{x}_{2i} + \gamma_{3i} L_{1i}^{1/3} |x_{1i} - \hat{x}_{1i}|^{2/3} \text{sign}(x_{1i} - \hat{x}_{1i}),\\ v_{2i} = \hat{x}_{3i} + \gamma_{2i} L_{1i}^{1/2} |v_{1i} - \hat{x}_{2i}|^{1/2} \text{sign}(v_{1i} - \hat{x}_{2i}),\\ v_{3i} = \gamma_{1i} L_{1i} \text{sign}(v_{2i} - \hat{x}_{3i})\end{cases} \tag{19}$$

where $\hat{x}_{1i}, \hat{x}_{2i}$, and $\hat{x}_{3i}$ are the estimates of x_{1i}, x_{2i}, and $\dot{x}_{2i}$, respectively. A possible parameters selection here is $\gamma_{3i} = 2, \gamma_{2i} = 1.5$, and $\gamma_{1i} = 1.1$, which can be referred to Levant (2003).

Define the estimation errors $e_{1i} = x_{1i} - \hat{x}_{1i}, e_{2i} = x_{2i} - \hat{x}_{2i}$, and $e_{3i} = \dot{x}_{2i} - \hat{x}_{3i}$. Then the error dynamics is governed by

$$I:\begin{cases}\dot{e}_{1i} = -\gamma_{3i} L_{1i}^{1/3} |e_{1i}|^{2/3} \text{sign}(e_{1i}) + e_{2i},\\ \dot{e}_{2i} = -\gamma_{2i} L_{1i}^{1/2} |e_{2i} - \dot{e}_{1i}|^{1/2} \text{sign}(e_{2i} - \dot{e}_{1i}) + e_{3i},\\ \dot{e}_{3i} = -\gamma_{1i} L_{1i} \text{sign}(e_{3i} - \dot{e}_{2i}) + x_{2i}^{(2)}.\end{cases} \tag{20}$$

It can be inferred from Levant (2003) that system (20) is finite-time stable under Assumption 2. That is, e_{1i}, e_{2i}, and $\dot{e}_{2i}$ will converge to zero when $t > T_{2i}$, e_{2i} and $\dot{e}_{2i}$ are bounded when $t \le T_{2i}$.

Define an additional uncertainty $\bar{H}_{di} = H_{di} - F_{2i} e_{2i} - \dot{e}_{2i}$. Assuming that E_i is the Lipschitz constant of the term $F_{2i} e_{2i} + \dot{e}_{2i}$, then $\bar{H}_{di}$ satisfies the Lipschitz condition with the Lipschitz constant $\bar{L}_{2i} = L_{2i} + E_i$. As such, the second HOSMO is designed to estimate $\bar{H}_{di}$ as follows

$$II:\begin{cases}\dot{\hat{\bar{x}}}_{2i} = v_{4i} + F_{ri}(x_{1i}, \hat{x}_{2i}) + b_i u_i, \dot{\hat{x}}_{4i} = v_{5i},\\ v_{4i} = \hat{x}_{4i} + \gamma_{2i} \bar{L}_{2i}^{1/2} |\hat{x}_{2i} - \hat{\bar{x}}_{2i}|^{1/2} \text{sign}(\hat{x}_{2i} - \hat{\bar{x}}_{2i}),\\ v_{5i} = \gamma_{1i} \bar{L}_{2i} \text{sign}(v_{4i} - \hat{x}_{4i})\end{cases} \tag{21}$$

where $\hat{\bar{x}}_{2i}$ and $\hat{x}_{4i}$ are the estimates of $\hat{x}_{2i}$ and $\bar{H}_{di}$. Define the estimation errors $\bar{e}_{2i} = \hat{x}_{2i} - \hat{\bar{x}}_{2i}$ and $e_{4i} = \bar{H}_{di} - \hat{x}_{4i}$, we can get similar error dynamics as (20). Then $\bar{e}_{2i}$ and e_{4i} will converge to zero after finite time T_{3i}. Moreover, when $t > \max\{T_{2i}, T_{3i}\}$, one can obtain that $\hat{\bar{x}}_{2i} = \hat{x}_{2i} = x_{2i}$ and $\hat{x}_{4i} = \bar{H}_{di} = H_{di}$.

Next, considering the sliding surface (13) and the control law (15) once again, we can modify x_{2i} and H_{di} by using $\hat{x}_{2i}$ and $\hat{x}_{4i}$, respectively. Naturally, the control law based on HOSMO is presented as

$$\begin{aligned} u_i &= -b_i^{-1}(u_{eqi} + u_{ni}),\\ u_{eqi} &= \frac{1}{k_i \alpha_i} |\hat{x}_{2i}|^{2-\alpha_i} \text{sign}(\hat{x}_{2i}) + F_{ri}(x_{1i}, \hat{x}_{2i}) + \hat{x}_{4i},\\ u_{ni} &= \lambda_{1i} \hat{s}_i + \lambda_{2i} |\hat{s}_i|^{\beta_i} \text{sign}(\hat{s}_i),\\ \hat{s}_i &= x_{1i} + k_i |\hat{x}_{2i}|^{\alpha_i} \text{sign}(\hat{x}_{2i}).\end{aligned} \tag{22}$$

Theorem 3. Under Assumption 2, considering the case that if the angular rate ω_i is the only available state, the observers and control law are designed as (19), (21) and (22), respectively, then it guarantees that the angular rate ω_i converges to the desired value ω_i^* in finite time.

Proof. The proof is divided into two steps. First, system variables $\hat{s}_i, x_{1i}$, and $\hat{x}_{2i}$ will not escape to infinity in finite time $\max\{T_{2i}, T_{3i}\}$. Second, system states x_{1i} and $\hat{x}_{2i}$ are finite-time stable.

Step 1: For the sliding mode variable $\hat{s}_i$ and system state $\hat{x}_{2i}$, taking their time derivatives yields

$$\begin{aligned} \dot{\hat{s}}_i =& \hat{x}_{2i} + e_{2i} + k_i \alpha_i |\hat{x}_{2i}|^{\alpha_i - 1} (\dot{x}_{2i} - \dot{e}_{2i})\\ =& -k_i \alpha_i |\hat{x}_{2i}|^{\alpha_i - 1}\\ & \times [\lambda_{1i} \hat{s}_i + \lambda_{2i} |\hat{s}_i|^{\beta_i} \text{sign}(\hat{s}_i) - e_{4i}] + e_{2i}\end{aligned} \tag{23}$$

and

$$\begin{aligned} \dot{\hat{x}}_{2i} =& -\frac{1}{k_i \alpha_i} |\hat{x}_{2i}|^{2-\alpha_i} \text{sign}(\hat{x}_{2i}) - \lambda_{1i} \hat{s}_i\\ & - \lambda_{2i} |\hat{s}_i|^{\beta_i} \text{sign}(\hat{s}_i) + e_{4i}.\end{aligned} \tag{24}$$

Define a finite time bounded function (Li and Tian, 2007) $V_2(\hat{s}_i, x_{1i}, \hat{x}_{2i}) = 1/2(\hat{s}_i^2 + x_{1i}^2 + \hat{x}_{2i}^2)$. Then taking the derivative of V_2 we have

$$\begin{aligned} \dot{V}_2 =& -k_i \alpha_i |\hat{x}_{2i}|^{\alpha_i - 1} (\lambda_{1i} \hat{s}_i^2 + \lambda_{2i} |\hat{s}_i|^{\beta_i + 1} - e_{4i} \hat{s}_i)\\ & + e_{2i} \hat{s}_i + x_{1i} (\hat{x}_{2i} + e_{2i}) - \frac{1}{k_i \alpha_i} |\hat{x}_{2i}|^{3-\alpha_i} - \lambda_{1i} \hat{s}_i \hat{x}_{2i}\\ & - \lambda_{2i} |\hat{s}_i|^{\beta_i} \text{sign}(\hat{s}_i) \hat{x}_{2i} + e_{4i} \hat{x}_{2i}\\ \le& k_i \alpha_i |\hat{x}_{2i}|^{\alpha_i - 1} |e_{4i}| |\hat{s}_i| + \frac{1}{2} e_{2i}^2 + \frac{1}{2} \hat{s}_i^2 + \frac{1}{2} {x_{1i}}^2\\ & + \frac{1}{2} \hat{x}_{2i}^2 + \frac{1}{2} {x_{1i}}^2 + \frac{1}{2} e_{2i}^2 + \frac{\lambda_{1i}}{2} \hat{s}_i^2 + \frac{\lambda_{1i}}{2} \hat{x}_{2i}^2\\ & + \lambda_{2i} |\hat{s}_i|^{\beta_i} |\hat{x}_{2i}| + \frac{e_{4i}^2}{2} + \frac{1}{2} \hat{x}_{2i}^2.\end{aligned} \tag{25}$$

Note that $|x|^\alpha < 1 + |x|$ when $0 < \alpha < 1$. With this property in mind, (25) can be further transformed into

$$\begin{aligned} \dot{V}_2 \le& \frac{(1 + \lambda_{1i} + \lambda_{2i} + 2k_i \alpha_i |e_{4i}|)}{2} |\hat{s}_i|^2 + x_{1i}^2\\ & + \frac{(2 + \lambda_{1i} + 2\lambda_{2i} + k_i \alpha_i |e_{4i}|)}{2} |\hat{x}_{2i}|^2\\ & + \frac{\lambda_{2i} + 2e_{2i}^2 + k_i \alpha_i |e_{4i}| + e_{4i}^2}{2}\\ \le& K_{V2} V_2 + L_{V2}\end{aligned} \tag{26}$$

where

$$\begin{aligned} K_{V2} =& \max\{1 + \lambda_{1i} + \lambda_{2i} + 2k_i \alpha_i |e_{4i}|,\\ & 2 + \lambda_{1i} + 2\lambda_{2i} + k_i \alpha_i |e_{4i}|\},\\ L_{V2} =& \max\{\frac{\lambda_{2i} + 2e_{2i}^2 + k_i \alpha_i |e_{4i}| + e_{4i}^2}{2}\}\end{aligned}$$

are bounded constants due to the boundness of e_{2i} and e_{4i} (Levant, 2003). From Li and Tian (2007) we can obtain that $\hat{s}_i, x_{1i}, \hat{x}_{2i}$ will not escape to infinity when $t \le \max\{T_{2i}, T_{3i}\}$.

Step 2: When $t > \max\{T_{2i}, T_{3i}\}$, from (20) we have $e_{2i} = e_{4i} = 0$. Then system (23) reduces to

$$\dot{\hat{s}}_i = -k_i \alpha_i |\hat{x}_{2i}|^{\alpha_i - 1} [\lambda_{1i} \hat{s}_i + \lambda_{2i} |\hat{s}_i|^{\beta_i} \text{sign}(\hat{s}_i)] \tag{27}$$

and the sliding surface reduces to

$$\hat{s}_i = x_{1i} + k_i |\dot{x}_{1i}|^{\alpha_i} \text{sign}(\dot{x}_{1i}). \tag{28}$$

The following steps are similar with (16)-(18). It can be proved that the system states x_{1i} and $\hat{x}_{2i}$ are finite-time stable with the control law (22). That is, the angular rate ω_i will converge to the desired value ω_i^* in finite time in the presence of both matched and unmatched uncertainties. This completes the proof.

4. SIMULATION RESULTS

To investigate the efficiency of the proposed output feedback control method, simulations on 2-DOF ISP system are performed, compared with the traditional PI controller. The parameters of the adopted PMDC motors are given as follows: $V_i = 24\text{V}$, $L_{ai} = 6.5\text{mH}$, $R_{ai} = 10.8\Omega$, $k_{ti} = 0.4\text{N}\cdot\text{m/A}$, $k_{vi} = 0.214\text{V/(rad/s)}$, $B_i = 7.4\times10^{-5}\text{N}\cdot\text{m}\cdot\text{s/rad}$, and the rated current $I_{Ni} = 2.5\text{A}$. The inertial matrices of gimbal system are given as

$$\mathbf{J_A} = \begin{bmatrix} 0.0583 & -0.0329 & -0.0468 \\ -0.0329 & 0.0897 & 0.0375 \\ -0.0468 & 0.0375 & 0.0621 \end{bmatrix} \text{kg}\cdot\text{m}^2,$$

$$\mathbf{J_K} = \begin{bmatrix} 0.0872 & -0.0253 & -0.0331 \\ -0.0253 & 0.0957 & 0.0416 \\ -0.0331 & 0.0416 & 0.1346 \end{bmatrix} \text{kg}\cdot\text{m}^2.$$

Suppose that the angular rate of vehicle motion or frame B is $\mathbf{\Omega_B} = [0, 25\sin 2\pi t, 25\cos 2\pi t]^{\text{T}}$ deg /s. The external lumped uncertain torque caused by the optical electronic tracker, cable restraint and wind gust are assumed to be $D_i(\omega_i, t) = [0.02\sin(\pi t) + 0.01]$ N·m.

For the pitch gimbal, the parameters of the proposed method are designed as $k_q = 1/45, \alpha_q = 1.5$, $\lambda_{1q} = 150, \lambda_{2q} = 100$, $\beta_q = 0.5, L_{1q} = 100$, and $\bar{L}_{2q} = 1\times10^4$. The parameters of PI controller are designed as $k_{pq} = 2$ and $k_{iq} = 15$. For the yaw gimbal, the parameters of the proposed method are designed as $k_r = 1/55, \alpha_r = 1.5$, $\lambda_{1r} = 200, \lambda_{2r} = 150$, $\beta_r = 0.5, L_{1r} = 100$, and $\bar{L}_{2r} = 5\times10^4$. The parameters of PI controller are designed as $k_{pr} = 5$ and $k_{ir} = 25$. The simulations are carried out under two operation modes, i.e., inertial stabilized mode and target tracking mode (Hurák and Řezáč, 2012).

4.1 Control Performance in Inertial Stabilized Mode

In the inertial stabilized mode, the control task is to keep LOS steady relative to inertial space in the presence of multiple disturbances. The initial values of angular rates q_a and r_a are set as 10 deg/s. The desired angular rate ω_i^* is set as 0. The simulation results in this case are shown in Figs. 1-2. It can be observed from Figs. 1-2 that both the virtual state x_{2i} and the lumped uncertainty H_{di} are precisely estimated in finite time by using HOSMOs. As shown in Fig. 1(c) and Fig. 2(c), the offsets of the inertial angular rate caused by disturbances are entirely removed by the proposed method, while it can only guarantee the system output converge to a region by PI controller and the bounded region also depends on the magnitude of the disturbances. From Fig. 3, one can see that the LOS is almost kept still in the steady-state even in the presence of multiple disturbances by the proposed method.

4.2 Control Performance in Target Tracking Mode

In the target tracking mode, the control task is to keep LOS toward a moving target. The initial values of angular rates q_a and r_a are set as 0. The desired angular rates are set as $\omega_q^* = 10\sin(\pi t)$ deg/s and $\omega_r^* = 10\cos(\pi t)$ deg/s. The simulation result is shown in Fig. 4. For simplicity, we only give the tracking path of LOS the in the yaw-pitch plane. It is obvious that the fast and accurate tracking is achieved with the proposed method.

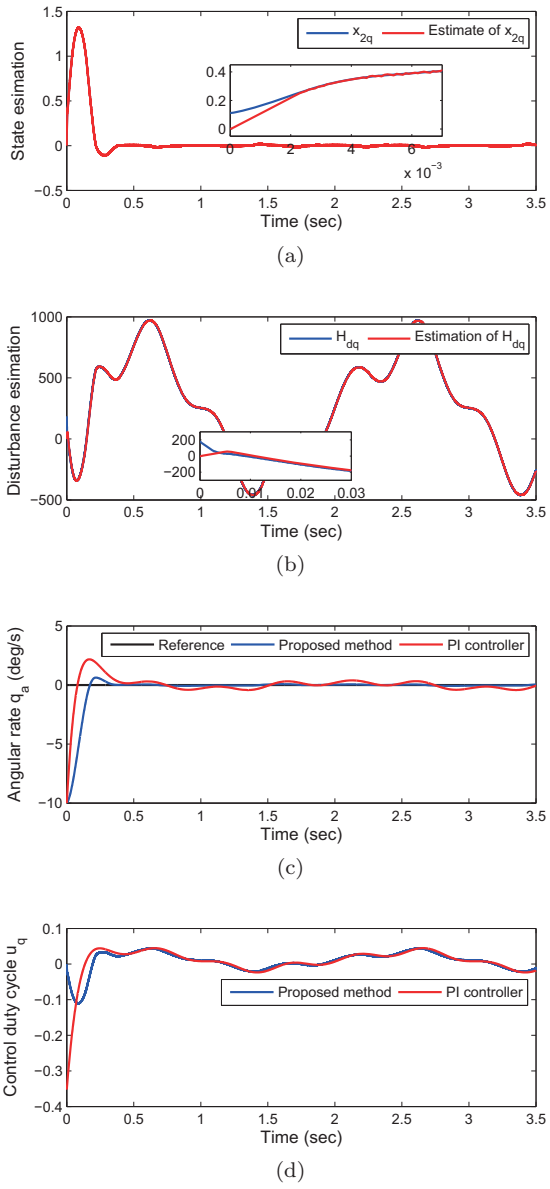

Fig. 1. Response curves of pitch gimbal: (a) Estimation of state x_{2q}, (b) Estimation of uncertainty H_{dq}, (c) Angular rate q_a, and (d) Control duty cycle u_q

5. CONCLUSION

The problem of output feedback stabilization for the ISP system subject to multiple unmatched disturbances in the current and angle sensorless case has been considered in this paper. Two HOSMOs have been designed to estimate the newly defined virtual state and the lumped uncertainty, respectively. A finite-time output feedback control has been developed. The comparative simulations have shown that finite-time convergence of inertial angular rate tracking error has been achieved even in the presence of multiple disturbances.

REFERENCES

Abdo, M., Vali, A., Toloei, A., and Arvan, M. (2014). Stabilization loop of a two axes gimbal system using self-tuning pid type fuzzy controller. *ISA Transactions*, 53(2), 591–602.

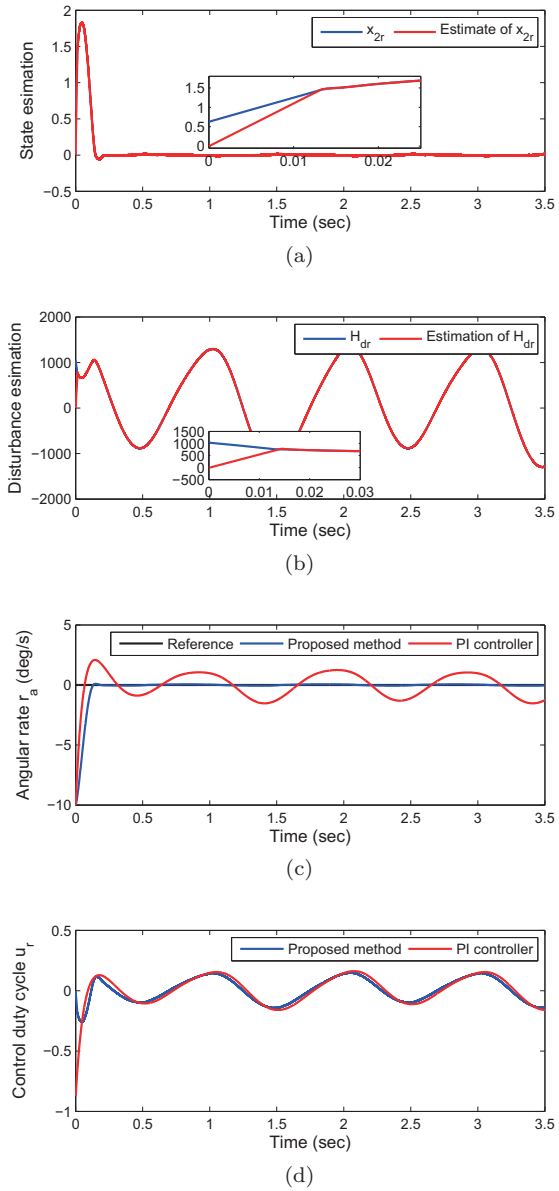

(a) (b) (c) (d)

Fig. 2. Response curves of yaw gimbal: (a) Estimation of state x_{2r}, (b) Estimation of uncertainty H_{dr}, (c) Angular rate r_a, and (d) Control duty cycle u_r

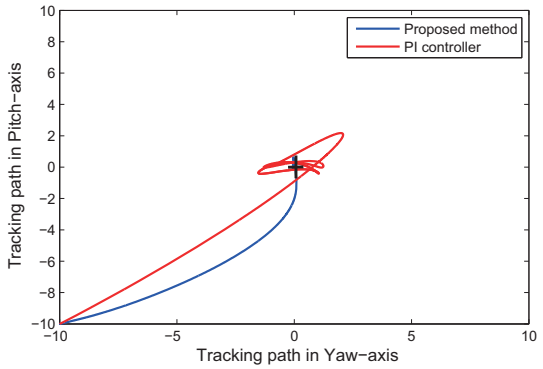

Fig. 3. Tracking path of LOS in the yaw-pitch plane under inertial stabilized mode

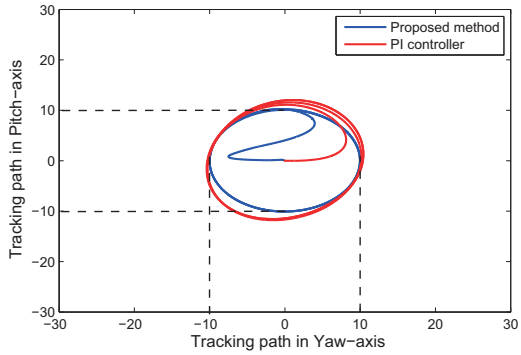

Fig. 4. Tracking path of LOS in the yaw-pitch plane under target tracking mode

Basin, M., Panathula, C., Shtessel, Y., and Ramírez, P. (2016). Continuous finite-time higher-order output regulators for systems with unmatched unbounded disturbances. *IEEE Transactions on Industrial Electronics*, 63(8), 5036–5043.

Chalanga, A., Kamal, S., Fridman, L.M., Bandyopadhyay, B., and Moreno, J.A. (2016). Implementation of super-twisting control: super-twisting and higher order sliding-mode observer-based approaches. *IEEE Transactions on Industrial Electronics*, 63(6), 3677–3685.

Chen, Z. and Huang, J. (2005). Global robust output regulation for output feedback systems. *IEEE Transactions on Automatic Control*, 51(1), 117–121.

Dai, C., Yang, J., Wang, Z., and Li, S. (2016). Universal active disturbance rejection control for non-linear systems with multiple disturbances via a high-order sliding mode observer. *IET Control Theory & Applications*. doi:10.1049/iet-cta.2016.0709.

Ekstrand, B. (2001). Equations of motion for a two-axes gimbal system. *IEEE Transactions on Aerospace and Electrononic System*, 37(3), 1083–1091.

Feng, Y., Yu, X., and Man, Z. (2002). Non-singular terminal sliding mode control of rigid manipulators. *Automatica*, 38(12), 2159–2167.

Hurák, Z. and Řezáč, M. (2012). Image-based pointing and tracking for inertially stabilized airborne camera platform. *IEEE Transactions on Control Systems Technology*, 20(5), 1146–1159.

Levant, A. (2003). Higher-order sliding modes, differentiation and output feedback control. *International Journal of Control*, 76(9/10), 924–941.

Li, S. and Tian, Y. (2007). Finite-time stability of cascaded time-varying systems. *International Journal of Control*, 80(4), 646–657.

Řezáč, M. and Hurák, Z. (2013). Structured mimo h∞ design for dual-stage inertial stabilization: case study for hifoo and hinfstruct solvers. *Mechatronics*, 23(8), 1084–1093.

Yu, S., Yu, X., Shirinzadeh, B., and Man, Z. (2005). Continuous finite-time control for robotic manipulators with terminal sliding mode. *Automatica*, 41(11), 1957–1964.

Zhou, X., Zhang, H., and Yu, R. (2014). Decoupling control for two-axis inertially stabilized platform based on an inverse system and internal model control. *Mechatronics*, 24(8), 1203–1213.